

## Liquid Flow through Defective Layered Membranes: A Phenomenological Description


Alexander Quandt,<sup>1</sup> Andrii Kyrylchuk<sup>1,2,3</sup>,<sup>ORCID</sup> Gotthard Seifert,<sup>4</sup> and David Tománek<sup>1,3,\*</sup>

<sup>1</sup>*Mandelstam Institute for Theoretical Physics and School of Physics, University of the Witwatersrand, 2050 Johannesburg, South Africa*

<sup>2</sup>*Institute of Organic Chemistry, National Academy of Sciences of Ukraine, Murmanska Str. 5, 02660 Kyiv, Ukraine*

<sup>3</sup>*Physics and Astronomy Department, Michigan State University, East Lansing, Michigan 48824, USA*

<sup>4</sup>*Theoretical Chemistry, Technische Universität Dresden, 01062 Dresden, Germany*

 (Received 7 July 2020; revised 10 August 2020; accepted 22 September 2020; published 21 October 2020)

We present a realistic phenomenological description of liquid transport through defective, layered membranes. We derive general expressions based on conventional models of laminar flow and extend the formalism to accommodate slip flow. We consider different types of defects including in-layer vacancies that provide an activation-free tortuous path through the membrane. Of the many factors that affect flow, the most important is the radius of in-layer vacancy defects, which enters in the fourth power in expressions for the flux density. We apply our formalism to water transport through defective multilayer graphene oxide membranes and find that the flow remains in the laminar regime. Our results show that observed high water permeability in this system can be explained quantitatively by a sufficient density of in-layer pores that shorten the effective diffusion path.

DOI: [10.1103/PhysRevApplied.14.044038](https://doi.org/10.1103/PhysRevApplied.14.044038)

### I. INTRODUCTION

Porous layered structures, in particular graphite oxide (GO) [1], have been claimed for a long time to bear special advantage for the purification of liquids, in particular the desalination of water. These initial claims have regained recent interest due to advances in the synthesis and characterization of such layered materials. This is particularly true for ordered hydrophilic multilayer GO (MLGO) [2], a new term coined for layered GO, which emerges as a very promising material for the separation of hydrated ions from water molecules. Since liquid flow has so far not been observed with subnanometer resolution, our understanding to date has relied almost exclusively on atomistic simulations. Only limited information is available about the microscopic structure and the flow mechanism of water molecules in-between layers of graphite [3,4] and GO [4–6]. Molecular dynamics (MD) simulations with parameterized force fields [7–10] and neutron diffraction studies [11] have provided valuable insight into the system, but significant controversies still remain regarding the microscopic mechanism of water transport through GO membranes. One of these involves a very high permeability of water in MLGO [12,13], which could be caused by a sufficient density of atomic-scale defects, or alternatively by

the presence of “graphene capillaries” that would cause an “ultrafast water flow” [12,14] through the membrane.

To obtain better insight into the matter, we have developed a phenomenological model that addresses all relevant aspects of liquid flow through a defective, layered membrane. Our approach is not system specific and considers different defect geometries. Using water flow through MLGO as an important example, we show how the microscopic structure of the membrane affects its hydraulic conductivity. With a sufficient density of in-layer vacancy defects, the effective diffusion path of water molecules through the membrane is relatively short and the resulting water permeability is high.

### II. FORMAL TREATMENT OF LIQUID FLOW THROUGH DEFECTIVE MEMBRANES

#### A. Phenomenological description of constrained laminar flow

The flux density  $q$  of a fluid passing through a porous membrane is given by the volume per unit area and time and has the dimension of velocity. For laminar flow, Darcy’s law finds this quantity to be proportional to the gradient  $\nabla p$  of the applied pressure  $p$ , as

$$q = -\frac{k}{\eta} \nabla p. \quad (1)$$

\*[tomanek@nanoten.com](mailto:tomanek@nanoten.com)

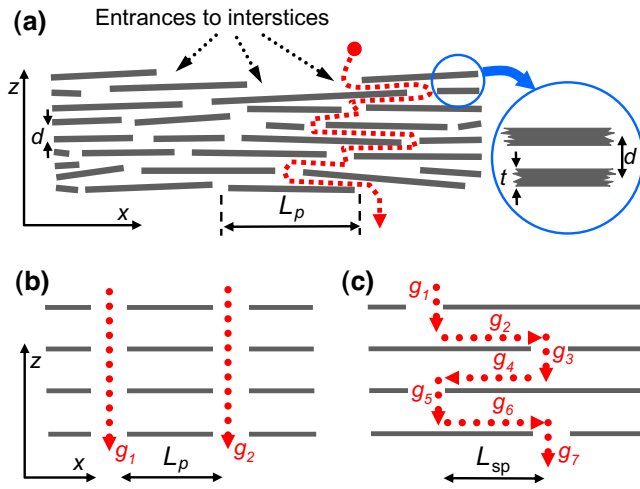


FIG. 1. Mechanism of liquid flow through a defective layered membrane. (a) Schematic route of a molecule, proposed by Boehm [1] for the representative case of  $\text{H}_2\text{O}$  passage through GO. The entrance to interstices occurs at the edge of a finite flake and proceeds through slit pores in-between layers of thickness  $t$ , separated by the average distance  $d$ . Here  $L_p$  is the average in-layer pore separation, with  $L_p \rightarrow \infty$  in a defect-free membrane. In-layer pores may be connected (b) in parallel and form channels that are separated by  $L_p$  and normal to the membrane, or (c) in series, forming tortuous channels in a staggered arrangement with lateral offset  $L_{sp}$ .

Here  $k$  describes the permeability of the membrane, a somewhat awkward quantity to model [15], and  $\eta$  is the dynamic viscosity of the fluid.

In analogy to Eq. (1) we can define the hydraulic conductivity  $g$  of a single membrane of finite thickness  $T$  using the general relation

$$q = g\Delta p, \quad (2)$$

where  $\Delta p$  is the pressure difference between the two sides of the membrane. Next we consider a complex layered membrane consisting of a network of pores forming a percolation path across the membrane, as seen in Fig. 1(a), which schematically shows the flow of water through GO. The standard approach [15] to model the permeability of this complex network of pores in a membrane is using a set of individual hydraulic conductivities  $g_n$  for laminar pipe flow, where the pipe-type pores are connected either in series or in parallel, as shown in Figs. 1(b) and 1(c). We note that conductivities  $g_n$  are different for in-layer pores and for “slit” pores in-between layers.

A parallel arrangement of pores, shown in Fig. 1(b), results in an effective hydraulic conductivity  $g_{\text{par}}$ , whereas an arrangement of pores in series, shown in Fig. 1(c),

yields the effective hydraulic conductivity  $g_{\text{ser}}$ . These effective hydraulic conductivities are given by

$$g_{\text{par}} = \sum_n g_n \quad (3)$$

and

$$g_{\text{ser}} = \left[ \sum_n g_n^{-1} \right]^{-1}. \quad (4)$$

For a particular system, these conductivities may be estimated using percolation models, scaling laws, and basic statistical assumptions [15].

The defective membrane as a whole can be considered as a parallel arrangement of pores that may vary in shape and density. Each pore with its individual shape then contributes  $Q_p$  to the total flux of the liquid through the membrane. The value  $Q_p(\vec{u})$  can be uniquely characterized by the parameter vector  $\vec{u}$  for each pore, where each individual component  $u_i$  describes a quantity related to  $Q_p$ . Such components may describe the spatial distribution of  $Q_p$  values along the  $x$  or  $y$  direction, or the distribution of specific factors characterizing the shape of a pore. Integration over the entire  $\vec{u}$  space should correctly account for all  $Q_p$  values found in the membrane with the correct probability distribution.

We define the areal density of pores by  $\rho_p = N_p/A$ , where  $N_p$  is the number of pores across the unit area  $A$ . In analogy to  $Q_p$ , an inhomogeneous areal density of pores can be defined by  $\rho_p(\vec{v})$ , where a particular distribution of relevant factors is described by vector components  $v_j$ . Also in this case, integration over the entire  $\vec{v}$  space should correctly cover all  $\rho_p$  values found in the membrane with the correct probability distribution. This provides us with a general expression for the flux density  $q$  through a nonuniform defective membrane

$$q = \frac{\int f(\vec{u})Q_p(\vec{u})g(\vec{v})\rho_p(\vec{v})d\vec{u}d\vec{v}}{\int f(\vec{u})g(\vec{v})d\vec{u}d\vec{v}} = \langle Q_p \cdot \rho_p \rangle, \quad (5)$$

where  $f(\vec{u})$  and  $g(\vec{v})$  are distribution functions and the denominator provides normalization. The purely descriptive integral expression in Eq. (5) does not make any assumptions about defects in terms of their density and type. It is the most general way to express the flux density across a membrane. Among others, it provides an adequate description of a membrane with a high density of narrow pores in one part and a low density of wide pores in a different part. The application of Eq. (5) to specific types of pores is addressed in the following.

In a membrane containing uniformly distributed identical pores,  $Q_p$  and  $\rho_p$  are constant, and the vector spaces  $\{\vec{u}\}$

and  $\{\vec{v}\}$  collapse to single points. This simplifies Eq. (5) to

$$q = Q_p \cdot \rho_p. \quad (6)$$

A standard porous membrane can be represented by a stack of infinite sheets with an even distribution of pores. The pores may be laterally offset by  $L_{sp}$  in the staggered configuration shown in Fig. 1(c), causing tortuous flow. The tortuosity  $\tau$  can be vaguely defined by the ratio between the total length  $L_{tot}$  of a molecular trajectory and the distance between its ends. Assuming a uniform pore distribution within a membrane containing  $N_l$  layers separated by the interlayer distance  $d$ , we find that

$$\tau = \frac{L_{tot}}{N_l d}. \quad (7)$$

We may further assume that the pores form a uniform triangular lattice in each layer. The lateral pore separation  $L_p$ , specified in Fig. 1(b), can then be estimated using

$$L_p = \left( \frac{2}{3^{1/2} \rho_p} \right)^{1/2}. \quad (8)$$

Further assuming an AB stacking of the triangular pore lattices in the layered system, the lateral offset of pores in adjacent layers, specified in Fig. 1(c), is  $L_{sp} = L_p / \sqrt{3}$ . With the total length of the shortest molecular path through the membrane given by  $L_{tot} = N_l(L_{sp} + d)$ , the tortuosity is given by

$$\tau = 1 + \frac{L_p}{\sqrt{3}d}. \quad (9)$$

Our considerations so far have been general, ignoring specific boundary conditions and the specific shape of the pores. Most descriptions of conventional viscous flow use the no-slip theorem, which means that the fluid adjacent to the walls of a constraint will have the same velocity as the wall.

### B. Tubular pores

There is one important pore shape, where the permeability is well understood, namely a cylindrical pipe of finite macroscopic length  $L_{tot}$  and radius  $R$ . As discussed in more detail in Appendix A, laminar flow through this pipe, subject to the no-slip theorem, is described well by the Hagen-Poiseuille law [15]

$$Q = -\frac{\pi R^4}{8\eta} \frac{\Delta p}{L_{tot}}. \quad (10)$$

Here  $Q$  describes the total flux, given by the total fluid volume passing through a cylindrical membrane per time, driven by the applied pressure difference  $\Delta p$ . Dividing

both sides of Eq. (10) by the cross section of the pipe, we obtain the flux density

$$q = -\frac{R^2}{8\eta} \nabla p. \quad (11)$$

Comparing this expression to Eq. (1), the permeability  $k_t$  of a membrane containing a single tubular pore of radius  $R$  is

$$k_t = \frac{1}{8} R^2. \quad (12)$$

As we show below, the tubular pore or modification thereof can also be used to describe fluid flow through nanoporous membranes. In particular, tortuous flow through the membrane may be represented by the flow through a multiply bent cylindrical pipe of total length  $L_{tot}$  in Eq. (10).

### C. Slit pores

A model alternative to a defective membrane is a defect-free, layered membrane of finite lateral extent  $L_{mem}$ . Laminar flow along a serpentine path through a membrane consisting of  $N_l$  parallel layers separated by  $d$  can also be described by the Hagen-Poiseuille law. The flux density in this case amounts to [16]

$$q_{sp} \approx \frac{d^4}{12L_{mem}^2 \eta} \frac{\Delta p}{N_l d}. \quad (13)$$

### D. Beyond the no-slip theorem

The validity of the no-slip theorem has been questioned in nanoporous materials [16,17]. During slip flow, molecules of the contained fluid may bounce along the walls of the steric constraint, with the distance between subsequent impacts being called the slip length. Interestingly, consideration of slip flow does not require a major revision of the theoretical framework presented so far [17].

We have summarized our basic considerations regarding slip flow in Appendix B. In the special case of slip flow in a liquid flowing through a cylindrical pipe, the expression for the flux  $Q$  in Eq. (10) needs to be modified to

$$Q = -\frac{\pi}{8\eta} [R^4 + L_s R^3] \frac{\Delta p}{L_{tot}}. \quad (14)$$

The first term in Eq. (14) is the flux of a viscous fluid through a pipe of radius  $R$  and length  $L_{tot}$  described in Eq. (10). The second term describes an additional flux component due to slippage, which is characterized by the slip length  $L_s$ .

## III. CHARACTERIZATION OF DEFECTIVE MODEL MEMBRANES

Among the typical defects in a membrane, which we consider here, are pores within individual layers that allow

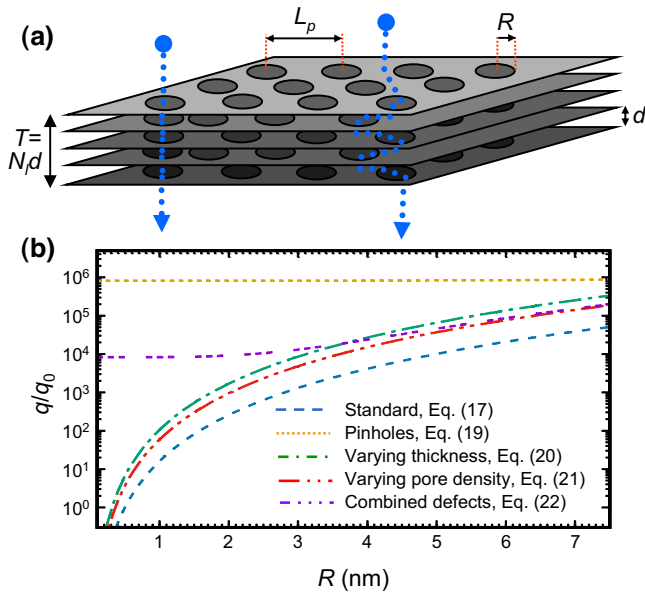


FIG. 2. Liquid flow through defective membranes. (a) Perspective view of a membrane containing  $N_l$  layers, separated by the distance  $d$ . Each layer contains round pores of radius  $R$  and average separation  $L_p$ . Straight flow through a “pinhole,” shown on the left, results from a straight arrangement of pores. Tortuous flow shown on the right results from a staggered arrangement of pores. (b) Liquid flow through defective layered membranes as a function of pore radius  $R$ . Specifics of each membrane are discussed in the text. Relative flux densities  $q/q_0$  are presented in units of the flux density  $q_0$  across a reference membrane containing pores with  $R = R_0 = 0.5$  nm. All results are for liquid water with viscosity  $\eta = 10^{-3}$  Pa s.

a liquid to flow through a membrane, as depicted in Figs. 1(b), 1(c), and 2(a). Among these, “pinhole defects,” shown in Figs. 1(b) and 2(a), provide the shortest path for liquid flow. We consider pores with a circular cross section that may display a uniform or nonuniform distribution of their radii  $R$ , tortuosity  $\tau$ , areal density  $\rho_p$ , and total liquid path length  $L_{\text{tot}}$ . A layered membrane, depicted in Fig. 2(a), will typically contain a combination of such defect variations that will affect the flux density. Knowing the distribution of each of these quantities, the flux density  $q$  can be estimated using integral (5). With the flux being proportional to  $R^4$  in Eq. (10), the pore radius plays the most critical role in the permeability of a membrane. Therefore, we present numerical flux densities in defective model membranes in Fig. 2(b) as a function of the pore radius. Since—depending on the defect densities and shapes—flux densities change by many orders of magnitude, they are presented on a logarithmic scale in Fig. 2(b).

### A. Reference membrane

What we call a “reference membrane” in Fig. 2 is a model structure closely related to approximately  $1 \mu\text{m}$

thick GO membranes studied by transmission electron microscopy (TEM). The reference membrane consists of layers containing round pores of radius  $R_0 = 0.5$  nm, arranged in a uniform triangular lattice with areal pore density  $\rho_p = \rho_0 = 0.25 \times 10^{15} \text{ m}^{-2}$ . The membrane consists of  $N_l = 1000$  layers separated by  $d = 1.2$  nm, a value typical of GO [18]. Using Eq. (8), we obtain the value  $L_p = 68.0$  nm for the lateral inter pore separation. Assuming an AB stacking of pore lattices in the layered system and using Eq. (9), we obtain  $\tau_0 = 33.7$  for the tortuosity of the shortest molecular path through the membrane. Combining Eqs. (6) and (10), the flux density of the reference membrane is

$$q_0 = -\frac{\pi R_0^4}{8\eta} \frac{\Delta p}{\tau_0 N_l d} \rho_p. \quad (15)$$

Using  $\eta = 10^{-3}$  Pa s for the viscosity of water and  $\Delta p = 1$  bar for a typical pressure difference between the two sides of the membrane, we find the reference flux density  $q_0 = -1.5 \times 10^{-11}$  m/s.

### B. Standard membrane

What we call a “standard membrane” in Fig. 2 is identical to the reference membrane with the exception that the pore radius  $R$  may vary. The flux density of the standard membrane is then

$$q_{\text{st}}(R) = -\frac{\pi R^4}{8\eta} \frac{\Delta p}{\tau_0 N_l d} \rho_p. \quad (16)$$

Comparing Eq. (16) to Eq. (15), we find a simple relationship between the flux densities of the standard and reference membranes

$$\frac{q_{\text{st}}(R)}{q_0} = \left(\frac{R}{R_0}\right)^4. \quad (17)$$

This relative flux density is shown in Fig. 2(b) for pore radii up to  $R = 7.5$  nm, the estimated average value for pores in GO [19].

### C. Membrane with pinholes

What we call a “membrane with pinholes” in Fig. 2 is a standard membrane with additional defects called “pinholes,” which cross the membrane in a straight line characterized by  $\tau_{\text{ph}} = 1$ . Our description follows experimental data for swelled GO membranes [20], to be discussed later, which contain up to micrometer-wide pinhole defects. We consider round pinholes with a constant radius  $R_{\text{ph}} = 2.5 \mu\text{m}$  and a constant density  $\rho_{\text{ph}} = 10^4 \text{ m}^{-2}$ . The flux density  $\Delta q_{\text{ph}}$  through a membrane with the parameters of the standard membrane that is free of any defects except

pinholes can be obtained using Eq. (16) and amounts to, in units of  $q_0$ ,

$$\frac{\Delta q_{\text{ph}}}{q_0} = \left(\frac{R_{\text{ph}}}{R_0}\right)^4 \frac{\rho_{\text{ph}}}{\rho_0} \tau_0. \quad (18)$$

The flux density through a standard membrane containing additional pinholes is then given by

$$\frac{q_{\text{ph}}(R)}{q_0} = \frac{q_{\text{st}}(R)}{q_0} + \frac{\Delta q_{\text{ph}}}{q_0}. \quad (19)$$

The constant quantity  $\Delta q_{\text{ph}}/q_0 = 0.82 \times 10^6$  is so large that it dominates over  $q_{\text{st}}(R)/q_0$  in the entire radius range considered in Fig. 2(b).

#### D. Membrane with varying thickness

The number of layers may not be the same across a defective layered membrane. Let us consider a standard membrane with  $N_l = 1000$  layers. A fraction  $\alpha$  of this membrane is much thinner, containing only  $N_{l,f}$  layers. Then, according to Eq. (10), the relative flux density will be

$$\frac{q_{\text{vt}}(R)}{q_0} = \frac{q_{\text{st}}(R)}{q_0} \left[ 1 + \alpha \left( \frac{N_l}{N_{l,f}} - 1 \right) \right]. \quad (20)$$

For  $\alpha = 30\%$  and  $N_{l,f} = 100$ , we obtain a 3.7 times higher flux density than for a standard membrane. This result is shown in Fig. 2(b).

#### E. Membrane with varying pore density

The areal density  $\rho_p$  of uniform pores may also vary across the membrane. Let us consider a standard membrane with  $\rho_p = \rho_0 = 0.25 \times 10^{15} \text{ m}^{-2}$ . In a fraction  $\beta$  of this membrane, the areal pore density  $\rho_{p,f}$  is different from the rest. In that case, according to Eq. (16), we obtain

$$\frac{q_{\text{vd}}(R)}{q_0} = \frac{q_{\text{st}}(R)}{q_0} \left[ 1 + \beta \left( \frac{\rho_{p,f}}{\rho_p} - 1 \right) \right]. \quad (21)$$

Assuming a local pore density increase by a factor of 15 in a fraction  $\beta = 40\%$  of the membrane, we find a flux density increase by a factor of 6.6 over the standard membrane. This result is shown in Fig. 2(b).

#### F. Membrane with a combination of defects

A typical membrane will contain a combination of defects. We consider a standard membrane with a fraction  $\alpha$  containing a different number of layers  $N_{l,f}$ , a fraction  $\beta$  containing a different pore density  $\rho_{p,f}$ , and a fraction

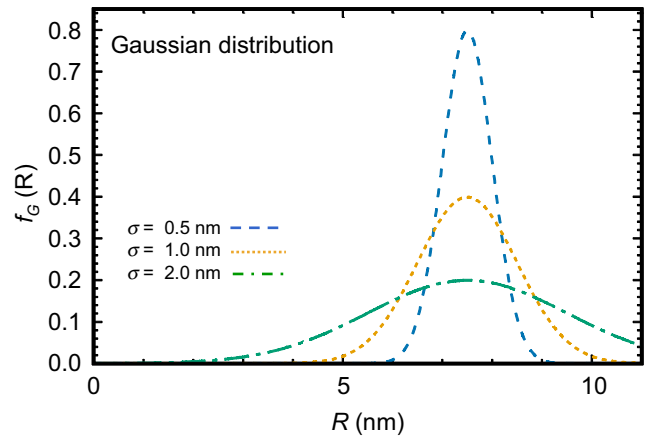


FIG. 3. Fraction of pores with specific radii represented by a Gaussian distribution defined in Eq. (23). Distributions are presented for the average radius  $\langle R \rangle = 7.5$  nm and different values of  $\sigma$ .

$\gamma$  containing pinholes, with  $\alpha + \beta + \gamma \leq 1$ . The relative flux density through such a membrane is given by

$$\begin{aligned} \frac{q_{\text{cd}}(R)}{q_0} = & \alpha \frac{q_{\text{vt}}(R)}{q_0} + \beta \frac{q_{\text{vd}}(R)}{q_0} + \gamma \frac{q_{\text{ph}}(R)}{q_0} \\ & + (1 - \alpha - \beta - \gamma) \frac{q_{\text{st}}(R)}{q_0}, \end{aligned} \quad (22)$$

where  $q_{\text{vt}}(R)/q_0$  is given by Eq. (20),  $q_{\text{vd}}(R)/q_0$  by Eq. (21), and  $q_{\text{ph}}(R)/q_0$  by Eq. (19). Results for such a membrane containing defect combination with  $\alpha = 30\%$ ,  $\beta = 40\%$ , and  $\gamma = 1\%$  are presented in Fig. 2(b).

#### G. Membrane with a Gaussian distribution of pore radii

For a constant value of the pore radius  $R$ , the relative flux density through a standard membrane is given by Eq. (16). We have to go back to Eq. (5) if the pore radii are not constant, but rather represented by a probability distribution function  $f(R)$ . In the following, we consider pores with a narrow distribution of radii around the mean value. A Gaussian or normal distribution of radii is described by

$$f_G(R) = \frac{1}{\sigma\sqrt{2\pi}} e^{-[(R-\langle R \rangle)/\sigma]^2/2}, \quad (23)$$

where  $\langle R \rangle$  is the average radius,  $\sigma$  is the standard deviation, and the full width at half maximum (FWHM) is  $2.355\sigma$ . The pre-exponential factor provides for normalization. Results for  $\langle R \rangle = 7.5$  nm and different values of  $\sigma$  are presented in Fig. 3.

The extension of Eq. (15) for the expectation value of the relative flux density in case of a Gaussian radius

TABLE I. Relative flux density through a standard membrane containing different distributions of round pores. Results presented are obtained using Eq. (24) for the Gaussian distribution and Eq. (26) for the Cauchy distribution of radii.

Gaussian distribution		Cauchy distribution	
$\sigma$ (nm)	$\langle q_{st}/q_0 \rangle$	$\nu$ (nm)	$\langle q_{st}/q_0 \rangle$
0.5	$5.2 \times 10^4$	0.5	$8.7 \times 10^8$
1.0	$5.6 \times 10^4$	1.0	$1.7 \times 10^9$
2.0	$7.3 \times 10^4$	0.1	$3.4 \times 10^9$

distribution is

$$\left\langle \frac{q_{st}}{q_0} \right\rangle = \frac{1}{R_0^4} \int_0^\infty f_G(R) R^4 dR, \quad (24)$$

where  $f_G(R)$  is expression (23) for a Gaussian distribution of radii. We evaluated the quantity  $\langle q_{st}/q_0 \rangle$  for the Gaussian distribution with  $\langle R \rangle = 7.5$  nm. Results for three different values of  $\sigma$  used in Fig. 3 are presented in Table I.

As expected, results of Eq. (24) converge to those of Eq. (17) for  $\sigma \rightarrow 0$ .

### H. Membrane with a Cauchy distribution of pore radii

Instead of the Gaussian distribution of radii  $f_G(R)$  defined in Eq. (15), we may consider the Cauchy distribution

$$f_C(R) = \frac{1}{\pi \nu \{1 + [(R - \langle R \rangle)/\nu]^2\}}, \quad (25)$$

where  $\langle R \rangle$  is the most probable radius and  $2\nu$  is the FWHM. This distribution carries more weight in the tails around  $\langle R \rangle$  than the Gaussian distribution. We show  $f_C(R)$  in Fig. 4 for  $\langle R \rangle = 7.5$  nm and different values of  $\nu$ .

The logical way to obtain the relative flux density through a standard membrane with a Cauchy radius distribution is to replace  $f_G(R)$  by  $f_C(R)$  in Eq. (24), leading to

$$\left\langle \frac{q_{st}}{q_0} \right\rangle = \frac{1}{R_0^4} \int_0^{R_{\max}} f_C(R) R^4 dR. \quad (26)$$

The important difference between Eqs. (24) and (26) is the upper limit of the integration range. Even though  $f_C(R)$  is normalized, its fourth moment diverges for  $R_{\max} \rightarrow \infty$ . We consider the finite value  $R_{\max} = 10^3$  nm large enough in comparison to  $\langle R \rangle$  to provide us with reasonable estimates of  $\langle q_{st}(R)/q_0 \rangle$  for the Cauchy distribution of radii.

Results for three different values of  $\nu$  used in Fig. 4 are presented in Table I. We note that flux densities are many orders of magnitude higher with the Cauchy distribution of radii than with the Gaussian distribution for the same value of  $\langle R \rangle$ .

## IV. RELEVANT EXAMPLE: GO MEMBRANE

### A. Morphology of a defective GO membrane

GO and MLGO membranes are considered excellent candidates for the filtration of liquids. MLGO is a highly aligned structure of layered GO, which consists of graphene layers that are chemically functionalized by epoxy-O and OH groups [1]. Unlike hydrophobic graphite and graphene, GO is hydrophilic and requires water for stabilization. The two commonly used approaches to synthesize GO are the Hummer [21] and the Brodie [22] processes. Both techniques yield an ordered material containing a substantial fraction of in-layer pores. Because of the intrinsic defective nature of GO, its designation as “graphene oxide” is, strictly speaking, a misnomer.

GO was introduced in the 1960s as a suitable material to form membranes that are particularly useful for water desalination based on reverse osmosis [1]. This material has been shown to find applications in the filtration and purification of not only water [23], but also other substances, which have to cross many pores in many layers.

A realistic structure of GO membranes, displayed schematically in Fig. 1(a), is very different from an ideal stack of two-dimensional (2D) layers and varies from sample to sample. Membranes should be considered a 3D system with a strong heterogeneity in the size, shape, and orientation of GO flakes that contain a variety of in-layer defects [20,24–27], including vacancies.

### B. Water transport through defective GO: merits of atomistic and phenomenological descriptions

A proper description of water transport through GO membranes is highly desirable, also to clarify the origin of the reported high flux density of water in these membranes

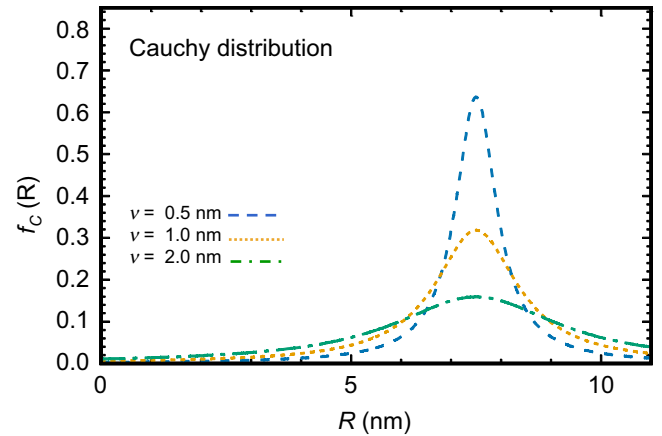


FIG. 4. Fraction of pores with specific radii represented by the Cauchy distribution defined in Eq. (25). Distributions are presented for  $\langle R \rangle = 7.5$  nm and different values of  $\nu$ .

[12,14]. The conventional description [1] of water transport through a porous multilayered GO membrane assumes a rather direct way of water molecules along the “slit” pores in-between GO flakes or through possible holes in the GO structure. The more recent alternative interpretation [12,13] of the high permeability of GO postulates a relatively long path, including transport along the inter-layer slit pores of the GO structure. According to the authors, a high water flow rate can then only be explained by introducing a fundamental mechanism called superpermeability. Key to this mechanism is so-called ultrafast flow of water through graphene nanochannels [12,14], which have been postulated to be present in GO membranes. These claims have been disputed to a large degree [28] based on microscopic structure studies of GO. Meanwhile, a number of experimental and theoretical studies have been published to better understand this rather exotic transport mechanism [14,16,29].

Because of the complexity of the problem, atomistic MD simulations have typically used empirical force fields that reproduce the structure of liquid water well, but usually failed to describe the interaction of water molecules with GO layers with the same accuracy. Yet it is exactly the interplay between water-water and water-GO interactions that is key to the understanding of water transport through pores in GO layers and even more along the slit pores. Moreover, as mentioned before, the realistic structure of defective GO is very complex. In that case, the predictive power of MD simulations addressing specific geometries is limited.

Under these circumstances, the phenomenological formalism in this study offers a viable alternative to describe water transport through GO membranes from a statistical viewpoint. This approach is based on well-established evidence that water properties, including viscosity and diffusion constants, are not changed during laminar flow through a nanopore. Also, the interaction between water molecules and GO layers does not change in a GO nanopore [4]. This approach offers a bias-free view of water flow through many types of tubular and slit pores that likely are present in the GO structure [28] and that have been discussed above.

### C. Scenarios of water transport through defective GO

#### 1. Tubular pores in GO

An insightful description of flow through nanoporous materials has been provided [17] for a membrane that is impermeable except for pores consisting of aligned carbon nanotube (CNT) arrays, which alone allow for the passage of fluid molecules. This corresponds to the case of hydraulic conductivities in parallel described by Eq. (3) and shown in Fig. 1(b). For a typical pressure difference  $\Delta p \approx 1$  bar between the two sides of the  $T = 1.2 \mu\text{m}$  thick GO reference membrane, we obtain  $|q| \approx |q_0| =$

$1.5 \times 10^{-11}$  m/s for the flux density when using the Hagen-Poiseuille expression (15) for laminar flow through round tubes in the absence of slip flow.

#### 2. Slit pores in GO

In case of lateral flow following a labyrinthine path through slit pores in-between defect-free GO layers, the flux density is described by Eq. (13). Using  $L_{\text{mem}} \approx 1 \mu\text{m}$  for the lateral extent of the layers in an otherwise defect-free reference membrane, we obtain  $q_{\text{sp}} \approx 1.4 \times 10^{-9}$  m/s.

Our estimated results for the flux density through tubular pores are six orders of magnitude and those for slit pores four orders of magnitude [16] lower than the measured flux densities of water in GO [12,14]. The discrepancy has been attributed to slip flow [12,14], with estimated slip lengths of the order of  $L_s \approx 0.1\text{--}1 \mu\text{m}$ . A viable alternative explanation for the difference, discussed in this paper, is based on the presence of in-layer defects that have been overlooked.

## V. DISCUSSION

The purpose of our study is to introduce a general heuristic framework to describe the flow of fluids through a membrane consisting of a defective layered material. Such membranes find an important application in separating unwanted substances from liquids. We focus on nanoporous GO membranes that bear promise for the desalination of water. Clearly, the same framework will also apply in many other cases.

The motivation for our study is the observation of high water flux rates through GO membranes and the controversy about their interpretation. We are especially disturbed by the discrepancy of several orders of magnitude between observed flux densities and our calculated values based on the assumption of laminar flow and the adequacy of the Hagen-Poiseuille law.

This is the reason why we use Occam’s razor approach to revisit all assumptions used in our modeling study. As discussed in Appendix A, there is no doubt that fluid flow in GO membranes is laminar and its description by the Hagen-Poiseuille law is adequate. The only remaining point in question is the presence and characteristics of defects.

Defects in the membrane structure may have been caused by severe damage that somehow went undetected. Pores in the structure may be more numerous or have different shapes than estimated. Since not all pores may be easily recognized in electron microscopy observations, pore densities obtained in such studies are likely underestimated. Additional uncertainty about realistic pore densities stems from the fact that microscopic pieces of the membrane used in microscopy may not be representative of the entire system.

Of all the factors that affect flow through defects most, we find that the pore radius  $R$  is by far the most important, since flux depends on  $R^4$ . It is quite likely that pore sizes have been underestimated, since pores are usually characterized by an electron microscope in dry samples. In the natural aqueous environment, water penetrates the membrane, swells it, and widens the pores. We note that increasing the pore radius  $R$  by a mere factor of 2 should increase the flux density by a factor of 16 according to the Hagen-Poiseuille law. Furthermore, swelling could increase the internal pressure within the membrane, but should not change the effect of the applied pressure  $\Delta p$  driving the flow.

Based on present experimental evidence, we believe that GO membranes are defective to a higher degree than previously admitted. Thus, we conclude that the significant discrepancy between observed high flux densities [12,14] and numerical values in our study can be explained simply using Hagen-Poiseuille law for laminar flow through different types of defects that either are not detected or their cross section is underestimated.

Other interpretations of the apparent discrepancy between theory and experiment have been discussed extensively in the literature [16,28,29], so that we may only offer a brief summary in the following.

Alternative interpretations of the observed “superfast” flow of “superfluid” water between GO sheets [12,13,30] are based on specific postulates regarding the microscopic structure of the membrane.

*Graphene capillaries*, consisting of large interconnected unoxidized areas of GO sheets [12,13,30,31], have been postulated to increase the flow of water through GO membranes. Even though the interlayer spacing  $d$  in graphite is only approximately 3.3 Å and thus much smaller than in GO,  $d$  has been postulated to increase significantly to approximately 7–7.5 Å in graphene capillaries located in oxidized areas. A large network of graphene capillaries was postulated to maintain slip flow of water and thus provide record-breaking permeability.

So far, however, there has been no independent evidence of such capillaries or even presence of pristine graphene in GO [28] based, among others, on high-resolution TEM imaging [25] and Raman spectra [32]. Presence of graphene capillaries should favor He permeation in water-free membranes rather than block it, as observed [12]. If graphene capillaries were present and important, permeation rates should depend on the flake sizes in laminates rather than being constant [33]. Also, the presence of hydrophobic graphene areas within GO should increase entry-exit barriers, which were specifically considered [34] and discussed [35] in the context of water transport through hydrophobic CNT-based membranes. It appears that a good strategy to maximize flow would be to reduce or eliminate activation barriers at the entrance and exit of water molecules. Such favorable conditions exist at

the edges of hydrophilic GO membranes that are free of pristine graphene.

An *ideal microscopic membrane* consisting of stacks of defect-free micrometer-sized GO layers at an approximately 0.7 nm interlayer distance was postulated as another important factor favoring “superfast” water flow [12]. However, it is well established that defects including pores and cracks are formed during sonication of GO, the preferred method for obtaining GO nanosheets [36]. This fact suggests that the postulate of a defect-free GO membrane is unrealistic.

Our own interpretation of the observed high permeation rate, based on what is known about GO membranes, their structure, and preparation, is much simpler: the high flow rate may be attributed to nanostructured defects that provide many short transport channels in parallel.

## VI. SUMMARY AND CONCLUSIONS

We have developed a realistic phenomenological description of liquid transport through defective, layered membranes. To do so, we have revisited the established formalism describing laminar flow and extended it to accommodate slip flow, a theoretical concept that would provide large corrections to laminar flow through defects. We applied the general expressions we derived to layered membranes containing a variety of defects that are not system specific. As a representative example, we chose layered GO, an important hydrophilic membrane system used for purification of water. Using realistic data for GO membranes, we estimated the force densities acting on water and found them to be insufficient to push the system out of the laminar regime, making the concept of slip flow redundant.

We found that in-layer vacancies, which prevail in defective GO, open a short, but tortuous path for activation-free transport of molecules through the membrane. Of the many factors that affect the flow, the most important is the radius of vacancy defects, which enters in the fourth power in the expression for the flux density based on the Hagen-Poiseuille law. In thin membranes with a sufficient density of such in-layer defects, the effective diffusion path of water molecules is relatively short and the water permeability increases significantly. We believe that a discrepancy of four orders of magnitude between observed water flow in GO membranes and calculated flux densities based on the Hagen-Poiseuille law are well explained by the presence of in-layer defects. In view of the fact that pores open up and swell in a membrane exposed to a liquid, electron microscopy observations on dry samples would typically underestimate the density and effective size of defects. This explains the significant increase in flow density without the need to invoke the presence of “graphene capillaries” that would enable an “ultrafast flow rate” of water.



## ACKNOWLEDGMENTS

D.T. acknowledges financial support by the NSF/AFOSR EFRI 2-DARE under Grant No. EFMA-1433459. A.Q. and D.T. acknowledge support by the Materials for Energy Research Group (MERG), the DST-NRF Center of Excellence in Strong Materials (CoE-SM) at the University of the Witwatersrand, the Mandelstam Institute for Theoretical Physics (MITP), and the Simons Foundation, Grant No. 509116. We appreciate valuable discussions with Alexandr Talyzin, Igor Baburin, and Dan Liu. Computational resources have been provided by the Michigan State University High Performance Computing Center.

A.Q., G.S., and D.T. conceived the idea. A.Q. and D.T. wrote the manuscript. A.K. researched the literature and performed selected calculations. D.T. finalized the manuscript with feedback from the other authors.

## APPENDIX A: LAMINAR FLOW THROUGH TUBULAR PORES

In the following we provide additional background information [37] used in the derivation of the Hagen-Poiseuille law describing laminar flux through a round pipe. We start our discussion with the most fundamental equation of fluid flow [38]

$$\vec{f} = \rho \frac{d\vec{v}}{dt}. \quad (\text{A1})$$

Here,  $\vec{f}$  is the net force per unit volume acting on the fluid of mass density  $\rho$  and velocity  $\vec{v}$ . Of course, Eq. (A1) is Newton's second law restated for a fluid. Since the problem of pipe flow is quasi-one-dimensional, we drop the vector notation in the following.

The right-hand side of Eq. (A1) represents the inertial force per volume  $f_i$ . The net force density  $f$  consists of a driving force density  $f_d$  and a viscous drag force density  $f_v$ . For a fluid flowing through a pipe with average velocity  $\langle v \rangle$ , the three forces can be estimated by [38]

$$f_i = \rho \frac{dv}{dt} \approx \rho \frac{\langle v \rangle^2}{L_{\text{tot}}} \quad (\text{A2})$$

and

$$f = f_d + f_v \approx -\frac{\Delta p}{L_{\text{tot}}} + \eta \frac{\langle v \rangle}{R^2}. \quad (\text{A3})$$

The meaning of all the other terms is the same as in Eq. (10).

We note that for nonvanishing  $f_i$ , the physics resulting from Eqs. (A1) and (A2) will be nonlinear due to the quadratic dependence of  $f_i$  on the average fluid velocity  $\langle v \rangle$ . As we show in the following,  $|f_i| \ll |f_d|, |f_v|$  under the conditions discussed here, so that the inertial force density may be neglected.

Let us first estimate the magnitude of the relevant force densities under the simplifying assumption that the average fluid velocity  $\langle v \rangle$  and the typical flux density  $q$  are of similar orders of magnitude. For water flow through a standard membrane with  $R = 1$  nm, described by Eq. (16), we obtain  $\langle v \rangle \approx |q_{\text{st}}| = 2.4 \times 10^{-10}$  m/s. According to Eq. (A2), the inertial force density  $f_i = \rho \langle v \rangle^2 / L_{\text{tot}} = 1.4 \times 10^{-12}$  N/m<sup>3</sup> if we use  $\rho = 10^3$  kg/m<sup>3</sup> for the density of water and  $L_{\text{tot}} = 40.4$   $\mu$ m for its tortuous path through the membrane. The viscous force density, defined in Eq. (A3), is  $|f_v| = \eta \langle v \rangle / R^2 = 2.4 \times 10^5$  N/m<sup>3</sup>. Considering the pressure difference  $\Delta p = 1$  bar between the two sides of the membrane, assumed for the reference membrane, and using Eq. (A3), we obtain  $|f_d| = \Delta p / L_{\text{tot}} = 2.4 \times 10^9$  N/m<sup>3</sup>. Since  $|f_i|$  is 17–21 orders of magnitude smaller than  $|f_d|$  and  $|f_v|$ , it can be safely neglected. This justifies our assumption that the flow through membranes we consider is well within the laminar regime. An independent confirmation of laminar flow obeying the Hagen-Poiseuille law at even higher pressure differences  $\Delta p = 6$  kbar has been provided by atomistic MD simulations of water flow through model nanopores [39].

Under steady-state conditions,  $f$  must vanish and we conclude that  $f_i \approx f = 0$ . Then, we may adopt some of the expressions presented above for the specific case of laminar flow through a round nanopipe. Assuming radial symmetry, the flow velocity  $v$  is described by the differential equation

$$\frac{1}{\eta} \frac{\Delta p}{L} = \frac{d^2 v}{dr^2} + \frac{1}{r} \frac{dv}{dr} = \frac{1}{r} \frac{d}{dr} \left( r \frac{dv}{dr} \right). \quad (\text{A4})$$

A general solution has the form

$$v(r) = \frac{1}{4\eta} r^2 \frac{\Delta p}{L} + C \ln(r) + D. \quad (\text{A5})$$

The values of parameters  $C$  and  $D$  are determined assuming axial symmetry and suitable boundary conditions at the walls. For conventional flow, the assumption of axial flow leads to  $dv/dr = 0$  at  $r = 0$  representing the center of the pipe. The no-slip condition at  $r = R$  at the wall implies that  $v(R) = 0$ .

Once parameters  $C$  and  $D$  are set, the flux  $Q$  may finally be obtained via a straightforward integration that leads to the Hagen-Poiseuille law

$$Q = \int_0^R 2\pi r v(r) dr = -\frac{\pi R^4}{8\eta} \frac{\Delta p}{L_{\text{tot}}}, \quad (\text{A6})$$

which is identical to Eq. (10).

## APPENDIX B: SLIP FLOW THROUGH TUBULAR PORES

In the case of slip flow, we have to abandon the no-slip condition  $v(R) = 0$ . Instead, we impose a alternative type

of boundary condition, which describes a scenario where the fluid molecules are bouncing along the walls of the pipe with the velocity

$$v(R) = L_s \frac{dv}{dr}(R). \quad (\text{B1})$$

Integrating over the radius with the modified boundary condition in Eq. (B1) leads to the expression

$$Q = -\frac{\pi}{8\eta} [R^4 + L_s R^3] \frac{\Delta p}{L_{\text{tot}}}, \quad (\text{B2})$$

which is identical to Eq. (14). Note that the slip length  $L_s$ , which occurs in this phenomenological boundary condition, is a parameter that may be freely adjusted to explain any observed deviation from the Hagen-Poiseuille law for laminar flow through a pipe.

- 
- [1] H. P. Boehm, A. Clauss, and U. Hofmann, Graphite oxide and its membrane properties, *J. Chim. Phys.* **58**, 141 (1961).
- [2] Inhwa Jung, Daniel A. Field, Nicholas J. Clark, Yanwu Zhu, Dongxing Yang, Richard D. Piner, Sasha Stankovich, Dmitriy A. Dikin, Heike Geisler, Carl A. Ventrice, and Rodney S. Ruoff, Reduction kinetics of graphene oxide determined by electrical transport measurements and temperature programmed desorption, *J. Phys. Chem. C* **113**, 18480 (2009).
- [3] Giancarlo Cicero, Jeffrey C. Grossman, Eric Schwegler, Francois Gygi, and Giulia Galli, Water confined in nanotubes and between graphene sheets: A first principle study, *J. Am. Chem. Soc.* **130**, 1871 (2008).
- [4] David Tománek and Andrii Kyrylchuk, Designing an All-Carbon Membrane for Water Desalination, *Phys. Rev. Appl.* **12**, 024054 (2019).
- [5] Mikhail V. Korobov, Aleksandr V. Talyzin, Anastasiya T. Rebrikova, Elizaveta A. Shilayeva, Natalya V. Avramenko, Alexander N. Gagarin, and Nikolay B. Ferapontov, Sorption of polar organic solvents and water by graphite oxide: Thermodynamic approach, *Carbon* **102**, 297 (2016).
- [6] Abhijit Gogoi, Tukhar Jyoti Konch, Kalyan Raidongia, and K. Anki Reddy, Water and salt dynamics in multi-layer graphene oxide (GO) membrane: Role of lateral sheet dimensions, *J. Membrane Sci.* **563**, 785 (2018).
- [7] A. Lerf, A. Buchsteiner, J. Pieper, S. Schöttl, I. Dekany, T. Szabo, and H. P. Boehm, Hydration behavior and dynamics of water molecules in graphite oxide, *J. Phys. Chem. Solids* **67**, 1106 (2006).
- [8] Ning Wei, Xinsheng Peng, and Zhiping Xu, Understanding water permeation in graphene oxide membranes, *ACS Appl. Mater. Interfaces* **6**, 5877 (2014).
- [9] Haiwei Dai, Zhijun Xu, and Xiaoning Yang, Water permeation and ion rejection in layer-by-layer stacked graphene oxide nanochannels: A molecular dynamics simulation, *J. Phys. Chem. C* **120**, 22585 (2016).
- [10] Shuping Jiao and Zhiping Xu, Non-continuum intercalated water diffusion explains fast permeation through graphene oxide membranes, *ACS Nano* **11**, 11152 (2017).
- [11] Alexandra Buchsteiner, Anton Lerf, and Jörg Pieper, Water dynamics in graphite oxide investigated with neutron scattering, *J. Phys. Chem. B* **110**, 22328 (2006).
- [12] R. R. Nair, H. A. Wu, P. N. Jayaram, I. V. Grigorieva, and A. K. Geim, Unimpeded permeation of water through helium-leak-tight graphene-based membranes, *Science* **335**, 442 (2012).
- [13] R. K. Joshi, P. Carbone, F. C. Wang, V. G. Kravets, Y. Su, I. V. Grigorieva, H. A. Wu, A. K. Geim, and R. R. Nair, Precise and ultrafast molecular sieving through graphene oxide membranes, *Science* **343**, 752 (2014).
- [14] Hubiao Huang, Zhigong Song, Ning Wei, Li Shi, Yiyin Mao, Yulong Ying, Luwei Sun, Zhiping Xu, and Xinsheng Peng, Ultrafast viscous water flow through nanostrand-channelled graphene oxide membranes, *Nat. Commun.* **4**, 2979 (2013).
- [15] Allen Hunt, Robert Ewing, and Behzad Ghanbarian, *Percolation Theory for Flow in Porous Media*, Lecture Notes in Physics, Vol. 880 (Springer International Publishing, Cham, ZG, Switzerland, 2014).
- [16] Yi Han, Zhen Xu, and Chao Gao, Ultrathin graphene nanofiltration membrane for water purification, *Adv. Funct. Mater.* **23**, 3693 (2013).
- [17] Jason K. Holt, Hyung Gyu Park, Yinmin Wang, Michael Stadermann, Alexander B. Artyukhin, Costas P. Grigoropoulos, Aleksandr Noy, and Olgica Bakajin, Fast mass transport through sub-2-nanometer carbon nanotubes, *Science* **312**, 1034 (2006).
- [18] Alexey Klechikov, Junchun Yu, Diana Thomas, Tiva Sharifi, and Alexandr V. Talyzin, Structure of graphene oxide membranes in solvents and solutions, *Nanoscale* **7**, 15374 (2015).
- [19] Justina Gaidukevič, Rasa Pauliukaitė, Gediminas Niaura, Ieva Matulaitienė, Olga Opuchovič, Aneta Radzevič, Gvidas Astromskas, Virginijus Bukauskas, and Jurgis Barkauskas, Synthesis of reduced graphene oxide with adjustable microstructure using regioselective reduction in the melt of boric acid: Relationship between structural properties and electrochemical performance, *Nanomaterials* **8**, 889 (2018).
- [20] Alexandr V. Talyzin, Tomas Hausmaninger, Shujie You, and Tamás Szabó, The structure of graphene oxide membranes in liquid water, ethanol and water-ethanol mixtures, *Nanoscale* **6**, 272 (2014).
- [21] William S. Hummers and Richard E. Offeman, Preparation of graphitic oxide, *J. Am. Chem. Soc.* **80**, 1339 (1958).
- [22] Benjamin Collins Brodie, XIII. On the atomic weight of graphite, *Phil. Trans. R. Soc. Lond.* **149**, 249 (1859).
- [23] Omid Akhavan and Elham Ghaderi, Toxicity of graphene and graphene oxide nanowalls against bacteria, *ACS Nano* **4**, 5731 (2010).
- [24] D. Pacilé, J. C. Meyer, A. Fraile Rodríguez, M. Papagno, C. Gómez-Navarro, R. S. Sundaram, M. Burghard, K. Kern, C. Carbone, and U. Kaiser, Electronic properties and atomic structure of graphene oxide membranes, *Carbon* **49**, 966 (2011).
- [25] Kris Erickson, Rolf Erni, Zonghoon Lee, Nasim Alem, Will Gannett, and Alex Zettl, Determination of the local chemical structure of graphene oxide and reduced graphene oxide, *Adv. Mater.* **22**, 4467 (2010).

- [26] Yongchao Si and Edward T. Samulski, Synthesis of water soluble graphene, *Nano Lett.* **8**, 1679 (2008).
- [27] Kian Ping Loh, Qiaoliang Bao, Goki Eda, and Manish Chhowalla, Graphene oxide as a chemically tunable platform for optical applications, *Nat. Chem.* **2**, 1015 (2010).
- [28] Alexandr Talyzin, Graphene oxide membranes: On the absence of “graphene capillaries,” “ultrafast flow rate” and “precise sieving,” [arXiv:1812.03941](https://arxiv.org/abs/1812.03941) (2018).
- [29] Young Hoon Cho, Hyo Won Kim, Hee Dae Lee, Jae Eun Shin, Byung Min Yoo, and Ho Bum Park, Water and ion sorption, diffusion, and transport in graphene oxide membranes revisited, *J. Membrane Sci.* **544**, 425 (2017).
- [30] Q. Yang, Y. Su, C. Chi, C. T. Cherian, K. Huang, V. G. Kravets, F. C. Wang, J. C. Zhang, A. Pratt, A. N. Grigorenko, F. Guinea, A. K. Geim, and R. R. Nair, Ultrathin graphene-based membrane with precise molecular sieving and ultrafast solvent permeation, *Nat. Mater.* **16**, 1198 (2017).
- [31] Jijo Abraham, Kalangi S. Vasu, Christopher D. Williams, Kalon Gopinadhan, Yang Su, Christie T. Cherian, James Dix, Eric Prestat, Sarah J. Haigh, Irina V. Grigorieva, Paola Carbone, Andre K. Geim, and Rahul R. Nair, Tunable sieving of ions using graphene oxide membranes, *Nat. Nanotechnol.* **12**, 546 (2017).
- [32] Patrick Feicht and Siegfried Eigler, Defects in graphene oxide as structural motifs, *Chem. Nano Mat.* **4**, 244 (2018).
- [33] Vivek Saraswat, Robert M. Jacobberger, Joshua S. Ostrander, Courtney L. Hummell, Austin J. Way, Jialiang Wang, Martin T. Zanni, and Michael S. Arnold, Invariance of water permeance through size-differentiated graphene oxide laminates, *ACS Nano* **12**, 7855 (2018).
- [34] Christophe Belin, Laurent Joly, and François Detcheverry, Optimal shape of entrances for a frictionless nanochannel, *Phys. Rev. Fluids* **1**, 054103 (2016).
- [35] Jens H. Walther, Konstantinos Ritos, Eduardo R. Cruz-Chu, Constantine M. Megaridis, and Petros Koumoutsakos, Barriers to superfast water transport in carbon nanotube membranes, *Nano Lett.* **13**, 1910 (2013).
- [36] Andrea Liscio, Konstantinos Kouroupis-Agalou, Xavier Diez Betriu, Alessandro Kovtun, Emanuele Treossi, Nicola Maria Pugno, Giovanna De Luca, Loris Giorgini, and Vincenzo Palermo, Evolution of the size and shape of 2D nanosheets during ultrasonic fragmentation, *2D Mater.* **4**, 025017 (2017).
- [37] Frank M. White, *Fluid Mechanics* (McGraw-Hill, New York, NY, USA, 2003).
- [38] Pierre-Gilles De Gennes, Françoise Brochard-Wyart, and David Quéré, *Capillarity and Wetting Phenomena* (Springer, New York, NY, USA, 2004).
- [39] Jacob Goldsmith and Craig C. Martens, Pressure-induced water flow through model nanopores, *Phys. Chem. Chem. Phys.* **11**, 528 (2009).